Chapter 2
Structure of Materials

In this chapter, we will briefly go through the hierarchical structure of materials. First, the atomic bonding and crystal structures are covered briefly. Then, the emphasis is placed on the presence of different types of defects and imperfections. Since point defects provide the fundamental basis for understanding the atomic mechanisms of diffusion, they are discussed in detail. In addition, the crystal structures including also the defect structures of intermediate phases and ordered binary intermetallics are quantitatively presented.

2.1 Hierarchical Structure of Materials

Most properties are actually highly structure sensitive. Therefore, it is of utmost importance to understand the basis for the structure of materials to be able to control the properties and reliability of engineering materials. Microstructure is a general term used to cover a wide range of structural features, ranging from those visible to the naked eye (for instance, macrostructure) to those corresponding to the inter-atomic distances in the crystal lattice (for instance, nanostructure). In other words, the size scale of the structural features ranges about 10 orders of magnitude. Therefore, in order to observe the structural features at these different scales, as shown in Fig. 2.1 [1], adequate resolving power is required.

Frequently, a large variety of structural features on different levels is noteworthy. Therefore, in the following chapters, the hierarchical structure of materials is presented.

2.2 Atomic Bonding

An atom can exist in different energy states according to the kind of interaction it has with neighboring atoms. The nature of this interaction is defined by the type of atomic bonding. The bonds can be categorized into two classes according to the bond energy. The primary bonds (>100 kJ/mol) are ionic, covalent, and metallic.

A. Paul et al., *Thermodynamics, Diffusion and the Kirkendall Effect in Solids*,
DOI: 10.1007/978-3-319-07461-0_2, © Springer International Publishing Switzerland 2014

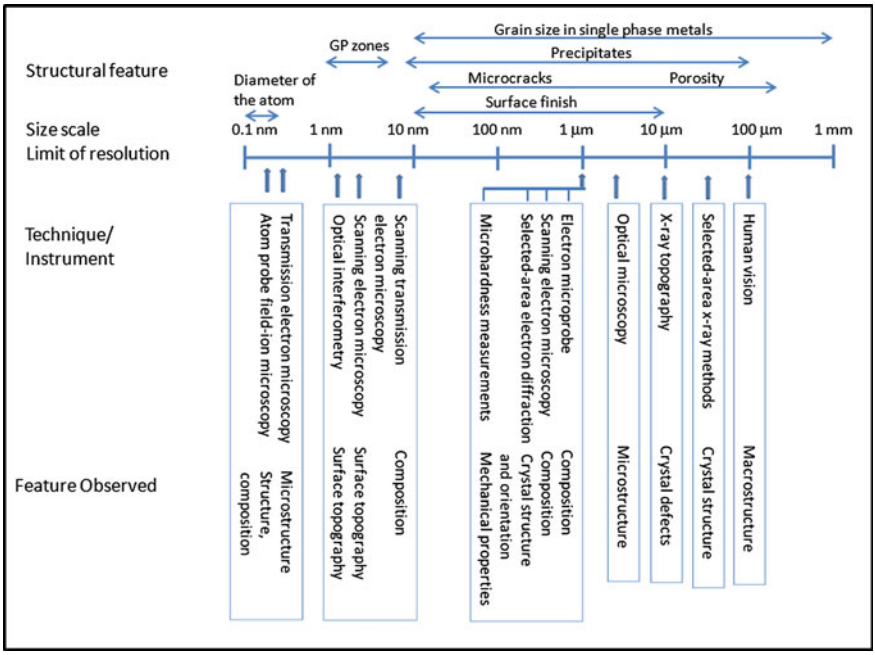

Fig. 2.1 Size scale relating structural features of metals to techniques of observation (redrawn from [1])

It is to be emphasized that in many materials, the bonding falls between these distinct categories. For example, the Si–O bond in silica is approximately half ionic and half covalent. The secondary bonds are of the van der Waals, or hydrogen, type. Many of the material properties, such as Young's modulus, the melting point, and the coefficient of thermal expansion (CTE) (as seen from Table 2.1), are related to the bond energy.

Ionically bonded crystals that possess high binding energies are generally considered to be hard, brittle, insulating, and thermally stable. The bond is based on the equilibrium between attractive and repulsive coulombic (electrostatic) forces. The ions are ordered in the crystal in such a non-directional manner that a macroscopically neutral material is generated. The structures typically have simple stoichiometry such as AB, AB_2, and A_2B.

Covalent crystals and molecules are based on bonds that share the pair of electrons in the direct line between the atoms. The directional bonding is caused by the concentrated electron density between the nuclei. Covalent bonding includes many types of interactions such as σ-bonding and π-bonding. These bonds can be either saturated, as in gas molecules H_2, N_2, O_2 …, or unsaturated, as in polymer's or covalent crystals C, Si, SiC …. Materials that possess bonds of a covalent nature are either insulators or semiconductors.

The nature of the atomic bond in metallic crystals differs from those of ionically and covalently bonded materials. The fundamentals of ionic and covalent bonds are

Table 2.1 Atomic bonding types, bonding energies, and respective melting temperatures for various substances

Bonding type	Substance	Bonding energy (kJ/mol)	Young's modulus (GPa)	CTE (10^{-6})	Melting temperature (°C)
Ionic	NaCl	640	39.98	44	801
	MgO	1,000	249	10.8	2,800
Covalent	Si	450	129	2.8	1,410
	C (diamond)	713	1,220	1.1	>3,550
Metallic	Hg	68		182	−39
	Al	324	69	23	660
	Fe	406	196	12	1,538
	W	849	344	4.5	3,410
Van der Waals	Ar	7.7			−189
	Cl_2	31			−101
Hydrogen	NH_3	35			−78
	H_2O	51	8.6–12 (ice)	51 (ice)	0

based on chemical valence. However, in metallic bonding, the theory enables the rationalization–typical metallic properties in addition to the aspect of the linking of atoms. By releasing the valence electrons the metal atoms in crystal can lower their energy state compared to individual atom. In this case the electrons are always close to nucleus (low potential energy region) but are not localized (i.e. cannot be associated with specific atom) so the kinetic energy is not increased too much. When summarized over the crystal this leadsto a stable structure. The bonds act between identical and different metallic atoms, as is revealed by the formation of numerous element and alloy structures. Typically, metallic atoms have either 8 or 12 neighboring atoms between which the bonds act. These resonating bonds usually permit plastic deformation and easy electron transfer throughout the structure.

2.3 Crystal Lattice

The formation of a crystal structure occurs as a result of bonding between atoms. Strong non-directional bonding typically allows atoms to pack efficiently, exhibiting planes of high atomic density containing close-packed directions. Crystals are thus solids in which all of the atoms occupy well-defined locations, being ordered across the whole material. These locations are defined by a crystal lattice, which is an infinite pattern of points, each of which having the same surroundings in the same orientation. Therefore, lattice is a mathematical concept out of which any point can be used as the origin for defining any other lattice points. There are only 14 possible three-dimensional lattices, called Bravais lattices, from which all crystal structures can be built as shown in Fig. 2.2.

It is to be noted that the crystal structure of a simple pure metal and that of a complex protein may both be described in terms of the same lattice, but the

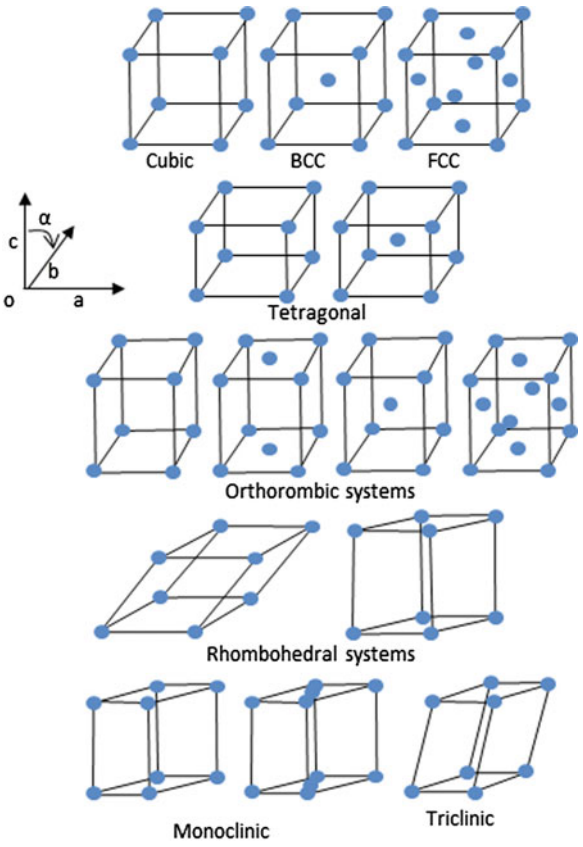

Fig. 2.2 Bravais lattices

number of atoms allocated to each lattice point (i.e., motifs) can vary from one to few thousands. Thus, a crystal structure is composed of a lattice plus a motif. The unit cells can be either simply primitive, body centered, face centered, or base centered. A primitive unit cell contains only a single lattice point, whereas a base-centered and body-centered cell contains two lattice points and a face-centered cell contains four lattice points.

The fundamentals of the crystal symmetry, planes, and directions as well as their indexing and nomenclature can be found from many excellent textbooks, for instance [2, 3]. Therefore, only the most common crystal types for pure metals and alloys, i.e., the close-packed face-centered cubic (FCC), body-centered cubic (BCC), and hexagonal close-packed (HCP) crystals, are presented in brief here. The atomic arrangement of the FCC and HCP crystals are shown in Fig. 2.3, where the location of the atom in the third layer defines whether the structure becomes hexagonal close packed (left, ABAB… arrangement) or FCC (right, ABCABC… arrangement). BCC crystals are not closely packed, and therefore, they contain more empty spaces (tetrahedral and octahedral interstitial sites) as can be seen from Fig. 2.4 and Table 2.2.

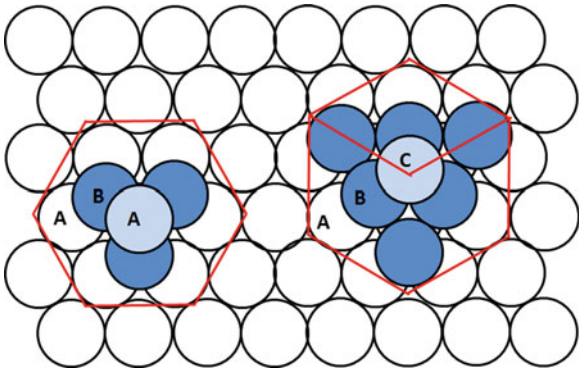

Fig. 2.3 Close-packed arrangements

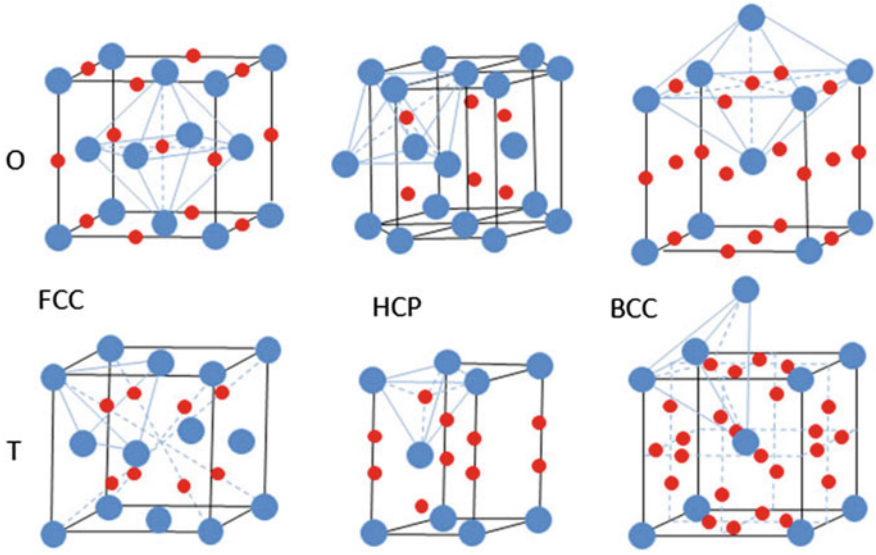

Fig. 2.4 Octahedral (*O*) and tetrahedral (*T*) interstitial sites in FCC-, HCP-, and BCC-type metals

2.4 Grain Structure

Grain structure is composed of small crystals that form a three-dimensional aggregate. The main characteristics are grain size, shape, and grain shape anisotropy. An impingement grain structure forms when grains grow until they meet or impinge, for example, during secondary recrystallization, producing characteristic ragged interfaces. A columnar grain structure is produced by unidirectional growth

Table 2.2 Number, location, and size of octahedral and tetrahedral sites in FCC, BCC, and HCP crystals [4]

Crystal structures	FCC	BCC	HCP
Number of atoms per unit cell	4	2	2
Coordination number of substitute atoms	12	8	12
Fraction of empty space	26.1 %	31.9 %	26.1 %
Octahedral sites	4	6	2
	0.414	155	0.414
	(1/2,0,0)	((1/2,0,0)	(1/3,2/3,1/4)
		(1/2,1/2,0)	
Number per unit cell	(1/2,1/2,1/2)		
Largest atom that fits in the site relative to the size of parent atom			
Coordinates that are reproduced by the symmetry			
Number of octahedral sites per parent atom	1	3	1
Coordination number of octahedral sites	12	8	12
Tetrahedral sites			
Number per unit cell			
Largest atom that fits in the site relative to the size of parent atom	8	12	4
Coordinates that are reproduced by the symmetry	0.225	0.291	0.225
	(1/4,1/4,1/4)	(1/2,1/4,0)	(1/3,2/3,1/8)
Number of tetrahedral sites per parent atom	2	6	2
Coordination number of tetrahedral sites	6	2	1
Closest packed planes and directions	{111}	{110}	{0001}
	<110>	<111>	<2110>
Typical metals having this structure	Al, Ni,	β-Ti,V,Cr	Mg, Zn, Cd,
	Cu, Ag,	Nb,	α-Ti, Zr,
	Au, Pb,γ-Fe,	Mo,W,	α-Co, Hf
	β-Co	α-Fe,Ta	

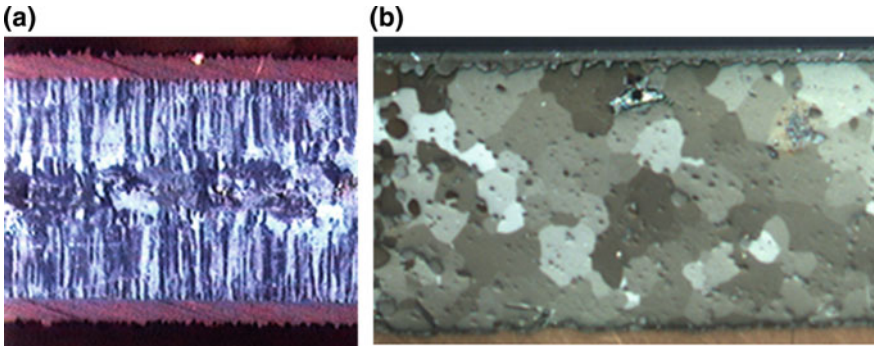

Fig. 2.5 Cross-polarized optical images from **a** columnar electrochemically plated Sn crystals between Cu equiaxed SnBi alloy and **b** recrystallized SAC solder interconnection after 3,000 cycles during a −40 °C ⟺ +125 °C thermal cycling test

such as in solidification or electrochemical plating (See Fig. 2.5a). Equiaxed grains can be formed by several processes such as recrystallization (See Fig. 2.5b) or solidification.

2.5 Defects

Many physical (especially mechanical) properties of solid materials are primarily based on the presence of different types of defects and imperfections. In other words, often specific material characteristics are deliberately fashioned by introducing a controlled amount of particular defect. The classification of crystalline imperfections is generally made according to either the geometry or dimensionality of the defect. Thus, the defects are typically divided into (i) point defects, which are related to a single or a few atomic positions, (ii) linear (or one-dimensional) defects, (iii) two-dimensional defects such as surfaces, interfaces, and different types of boundaries, and (iv) volume defects including inclusions, cracks, voids, and pores.

2.5.1 Point Defects

Point defects are central to gain an understanding of the atomic mechanisms of diffusion, and therefore, they are discussed in detail. There can be a few types of point defects present in the structure in an equilibrium condition (e.g., vacancies, impurities, and antistructure). Typically, in "pure" elements, vacancies and impurities are present in the structure. First, let us discuss the defects present in the pure elements and then turn to consider the defects present in the ordered phases.

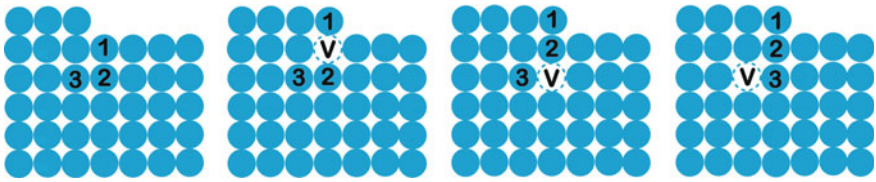

Fig. 2.6 Movement of atoms to create a vacancy at the interior

2.5.1.1 Equilibrium Vacancy Concentration in Pure Elements

The presence of vacancies in a pure element can be estimated using the same kind of treatment as was followed to find the free energy in a binary system, as explained previously in Sect. 1.8. The formation of vacancies can be explained, as shown in Fig. 2.6, where one atom diffuses from the interior of the crystal to the surface leaving a vacant site (the Schottky defect). There is another type of point defect, called the Frenkel defect, which is formed when an atom from a lattice site moves into an interstitial site thus leaving an empty space (vacancy) behind. For the sake of analysis, the presence of vacancies (V) in the element A can be visualized as a binary system of A and V. Now, the creation of vacancies is associated with the increase in internal energy because of broken bonds around the vacancies. In general, the equilibrium number of vacancies is so small that we can neglect the interaction between them. Thus, if we consider that the number of vacancies to be very small, then the increase in enthalpy resulting from the formation of vacancies can be written as

$$\Delta h \approx X_v \Delta h_v \tag{2.1}$$

Here, ΔX_v is the mole fraction of the vacancy and Δh_v is the increase in enthalpy caused by one mole of vacancies.

Factors contributing to Δh_v in metals are as follows:

1. Change in the volume. When an atom is removed from the center of the lattice and is placed at the surface, there is no change in the surface area, but rather an increase in the volume. This decreases the average energy of the electrons, giving a negative change in energy.
2. The removal of an atom leaves behind one atomic volume devoid of charge. Free electrons around the site tend to flow into this vacancy. Since there in no positive charge in the vacant site, the electrostatic energy is increased. To minimize this effect, there will be a sharp change in the electron density, which imposes in the end a higher kinetic energy for the electrons and an increase in the energy of the lattice.
3. When an atom is removed, the surrounding ions will relax into the vacancy decreasing slightly the energy of the final lattice.

If we now consider the total effect of all the above-mentioned three contributions, it is to be found that the sum is positive Δh_v; thus, it costs energy to form a vacancy.

The entropy can be divided into two parts, namely thermal entropy and configurational entropy (Sect. 1.5). Now, if we consider the change in entropy resulting from the mixing of vacancies with the pure element, there will be two types of contributions. First, there will be the change in the vibration pattern of the atoms next to vacancies because of extra free space. The increase in entropy caused by the extra freedom of vibration can be written as $X_v \Delta s_v$. Here, Δs_v is the increase in entropy for one mole of vacancies. Furthermore, there will be a change in configurational entropy considering the mixing of A and V and this can be expressed as (Note that we are considering $X_A + X_v = 1$)

$$\Delta s_{\text{mix}} = -R[X_v \ln X_v + (1 - X_v) \ln(1 - X_v)] \tag{2.2}$$

So the total change in entropy can be written as

$$\Delta s = \Delta s_v X_v - R[X_v \ln X_v + (1 - X_v) \ln(1 - X_v)] \tag{2.3}$$

Thus, the total free energy of the system containing vacancies can be written as

$$G = G_A + \Delta G \tag{2.4}$$

where G_A is the free energy of the defect free system of pure element A. ΔG is the change in free energy and can be expressed as (Sect. 1.3)

$$\Delta G = \Delta H - T\Delta S \tag{2.5}$$

From Eqs. 2.2 to 2.5, the total free energy of the system can be written as

$$G = G_A + X_v \Delta H_v - T\{\Delta S_v - R[X_v \ln X_v + (1 - X_v) \ln(1 - X_v)]\} \tag{2.6}$$

The change in enthalpy, entropy, and free energy due to an increasing number of vacancies can be seen in Fig. 2.7. It is apparent that ΔH increases linearly with the increase in vacancies, whereas $-T\Delta S$ decreases very rapidly in the beginning, but the rate of change decreases drastically. So it should be clear that in the beginning, the total free energy of the system will decrease with the creation of vacancies, but after a certain range, the free energy will start to increase because ΔH will start dominating. The system will therefore go through a minimum. We have seen before in Sect. 1.2 that a system will stay in equilibrium when it has minimum free energy. So we can state that the system will remain in equilibrium with free energy G_e. Further, we know that in the equilibrium condition,

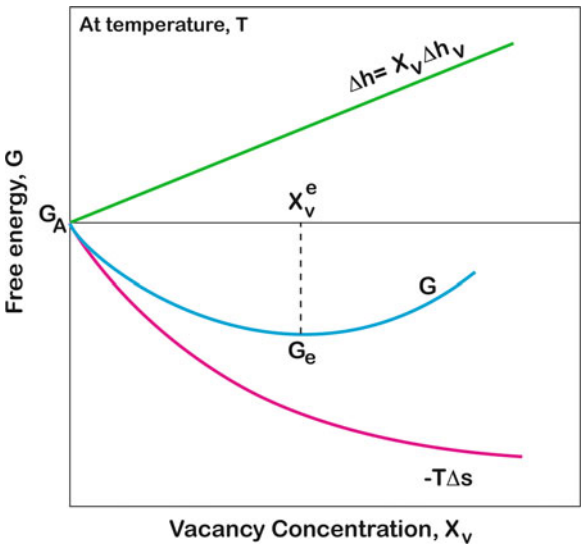

Fig. 2.7 The change in free energy of element A with the increase in vacancy concentration

$$\frac{dG}{dX_v} = 0 \tag{2.7}$$

So from the differentiation of G (Eq. 2.6) with respect to X_v and then by equaling it to zero, we can write

$$\Delta H_v - T\Delta S_v + RT\left[\ln X_v + X_v \cdot \frac{1}{X_v} - \ln(1 - X_v) - (1 - X) \cdot \frac{1}{(1 - X_v)}\right] = 0 \tag{2.8}$$

Since the number of vacancies that can be present in the system is very small, we can write $1 - X_v \approx 1$. Thus, Eq. 2.8 can be written as

$$\Delta H_v - T\Delta S_v + RT \ln X_v = 0 \tag{2.9}$$

So the relation for the equilibrium concentration of vacancies can be written as

$$X_v^e = X_v = \exp\left(-\frac{\Delta H_v - T\Delta S_v}{RT}\right) = \exp\left(-\frac{\Delta G_v}{RT}\right) \tag{2.10}$$

Here, X_v^e is the equilibrium concentration of vacancies at a particular temperature T, and ΔG_v is the activation energy for the formation of one mole of vacancies. Equation 2.10 can further be written as

$$X_v^e = X_v^0 \exp\left(-\frac{\Delta H_v}{RT}\right) \tag{2.11}$$

where ΔH_v is the activation enthalpy for the formation of vacancies and X_v^0 is the pre-exponential factor and is equal to

$$\exp\left(\frac{\Delta S_v}{R}\right) \tag{2.12}$$

It is to be noted here that if the vacancies are not present in their equilibrium fraction in a binary system, their chemical potential is not zero, and thus, it will transform the system essentially into a ternary one where, for instance, there is now more than one thermodynamic factor (Sect. 1.15).

2.5.1.2 Equilibrium Concentration of Impurities in Pure Elements

In many metals, especially in transition metals, interstitial atoms such as carbon, nitrogen, oxygen, and hydrogen can be present depending, to a large extent, on the metal. The presence of these impurities can change the properties of the material drastically. The maximum concentration of interstitial atoms that can be present depends on different factors such as the crystal structure of the metal and the size of the interstitial atoms. There are mainly two types of interstitial sites present in the structure: tetrahedral (surrounded by four solvent atoms) and octahedral (surrounded by six solvent atoms). However, since it has been observed that interstitial atoms typically prefer to occupy octahedral interstices (hydrogen is a known exception), we shall mainly consider this type of sites. The treatment to calculate the maximum solubility of interstitial atoms is slightly different to the treatment that was followed in the previous section to calculate vacancy concentration. This is because these atoms will occupy interstitial positions without displacing metal atoms which occupy normal lattice positions. To explain the treatment, let us first consider an element A, which has a BCC crystal structure and the presence of interstitial atoms, I, as shown in Fig. 2.8a. Possible octahedral interstitial positions in the BCC lattice are shown by black dots. In general, the size of the interstitial atoms is larger than the size of the interstitial site and furthermore, it cannot be smaller. So if any interstitial atom is present, the surrounding lattice will be strained. This means that the enthalpy of the system will be increased. If the increase in enthalpy resulting from the addition of one mole of interstitial atoms is Δh_I, then the total enthalpy increment of the system is expressed by

$$\Delta h = X_I \Delta h_I \tag{2.13}$$

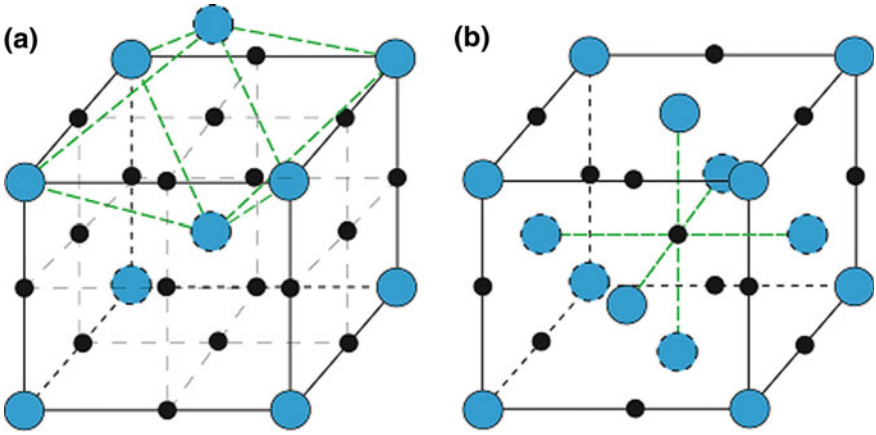

Fig. 2.8 Octahedral interstitial positions are shown by black dots in **a** BCC unit cell and **b** FCC unit cell

where $X_I = \frac{n_I}{N_0}$ is the mole fraction of the interstitial atoms present in the system and n_I is the total number of interstitial atoms. Again, there will be two different types of contribution to entropy. The first contribution comes from the fact that the vibration of atoms A next to the interstitial atoms will change from a normal mode of vibration and will be more random and irregular because of the distortion of the lattice. If we consider that the change of the entropy due to the change of vibration pattern is ΔS_I for one mole of interstitial atoms, then for X_I mole of interstitial atoms the change in entropy will be $X_\mathrm{I}\Delta S_\mathrm{I}$. Further, there will also be an increase in entropy because of the mixing of the solvent and interstitial atoms. Now, from the crystal structure, as shown in Fig. 2.8a for two solvent atoms, there are six sites for interstitial atoms. Additionally, we can write that for each A atom, there are three sites for interstitial atoms. So if we consider that there are N_0 numbers of A atoms, then there will be $3N_0$ numbers of sites available for interstitial atoms. In another sense, we can say that n_I atoms will randomly occupy n_I sites from $3N_0$ sites. Following statistical thermodynamics, the entropy of mixing can be written as

$$\Delta S_\mathrm{mix} = S - S_0 = k \ln w - k \ln 1 = k \ln w \tag{2.14}$$

where w is roughly the measure of randomness, S_0 is the entropy before mixing, and S is the entropy after mixing. Since in the case of a pure element, there is only one way by which atoms can be arranged, we can write $w = 1$. If we consider that interstitial atoms will choose their sites completely randomly, then we can write

$$w = \frac{3N_0!}{n_\mathrm{I}!(3N_0 - n_\mathrm{I})!} \tag{2.15}$$

According to Stirling's approximation,

$$\ln N! = N\ \ln N - N$$

Following Stirling's approximation, Eq. 2.15 can be derived as

$$\Delta S_{\text{mix}} = k[3N_0\ \ln 3N_0 - n_{\text{I}}\ \ln n_{\text{I}} - (3N_0 - n_{\text{I}})\ \ln(3N_0 - n_{\text{I}})] \tag{2.16}$$

Furthermore, Eq. 2.16 can be written as

$$\begin{aligned} \Delta S_{\text{mix}} &= R\left[3\ln 3N_0 - \frac{n_{\text{I}}}{N_0}\ln n_{\text{I}} - \frac{3N_0 - n_{\text{I}}}{N_0}\ln(3N_0 - n_{\text{I}})\right] \\ \Delta S_{\text{mix}} &= R\left[3\ln\frac{3N_0}{3N_0 - n_{\text{I}}} - \frac{n_{\text{I}}}{N_0}\ln\frac{n_{\text{I}}}{3N_0 - n_{\text{I}}}\right] \end{aligned} \tag{2.17}$$

Further, replacing $X_{\text{I}} = n_{\text{I}}/N_0$, Eq. 2.17 can be written as

$$\Delta S_{\text{mix}} = R\left[3\ln\frac{3}{3 - X_{\text{I}}} - X_{\text{I}}\ln\frac{X_{\text{I}}}{3 - X_{\text{I}}}\right] \tag{2.18}$$

So the total free entropy change can be written as

$$\Delta S = X_{\text{I}}\Delta S_{\text{I}} + R\left[3\ln\frac{3}{3 - X_{\text{I}}} - X_{\text{I}}\ln\frac{X_{\text{I}}}{3 - X_{\text{I}}}\right] \tag{2.19}$$

Moreover, the total free energy of the system after the addition of interstitial atoms can be written as

$$\begin{aligned} G &= G_A + \Delta G = G_A + \Delta H - T\Delta S_{\text{I}} \\ G &= G_A + X_{\text{I}}\Delta H_{\text{I}} - TX_{\text{I}}\Delta S_{\text{I}} - RT\left[3\ln\frac{3}{3 - X_{\text{I}}} - X_{\text{I}}\ln\frac{X_{\text{I}}}{3 - X_{\text{I}}}\right] \end{aligned} \tag{2.20}$$

As we have seen in the previous section that the equilibrium concentration of interstitial atoms can be found from $\frac{dG}{dX_{\text{I}}} = 0$. Thus,

$$\begin{aligned} &\Delta H_{\text{I}} - T\Delta S_{\text{I}} - RT\left[-\frac{3}{3 - X_{\text{I}}} - \frac{X_{\text{I}}}{X_{\text{I}}} - \ln X_{\text{I}} + \ln(3 - X_{\text{I}}) - \frac{X_{\text{I}}}{3 - X_{\text{I}}}\right] = 0 \\ &\Delta H_{\text{I}} - T\Delta S_{\text{I}} + RT\ \ln\frac{X_{\text{I}}}{3 - X_{\text{I}}} = 0 \end{aligned} \tag{2.21}$$

Further, the activation energy for the interstitial atom additions can be written as $\Delta g_{\text{I}} = \Delta H_{\text{I}} - T\Delta S_{\text{I}}$. Since we have considered that the concentration of impurities is much less, we can write $3 - X_{\text{I}} \approx 3$. So Eq. 2.21 can be written as

$$X_I = 3\exp\left(-\frac{\Delta g_I}{RT}\right) \tag{2.22}$$

Similarly, if we consider the FCC crystal, as shown in Fig. 2.8b, then the number of octahedral sites available for interstitial atoms is four. Further, in an FCC unit cell, the total number of atoms per unit cell is likewise four. So we can say that for N_0 solvent atoms, there will be N_0 sites available for interstitial atoms. As in the previous example, if we consider n_I interstitial atoms which will occupy randomly N_0 sites, then we can show that

$$X_I = \exp\left(-\frac{\Delta g_I}{RT}\right) \tag{2.23}$$

So in general, we can write that the equilibrium concentration of interstitial impurities present is

$$X_I = B\ \exp\left(-\frac{\Delta g_I}{RT}\right) \tag{2.24}$$

Here, factor B depends on the crystal structure.

Furthermore, Eq. 2.24 for any kind of crystal structures can be written as

$$X_I = X_I^0 \exp\left(-\frac{\Delta h_I}{RT}\right) \tag{2.25}$$

where ΔH_I is the activation enthalpy for interstitial impurities and X_I^0 is the pre-exponential factor which is defined as

$$X_1^\circ = B\ \exp\left(\frac{\Delta s}{R}\right). \tag{2.26}$$

In above examples, we have seen that a BCC crystal has a higher number of octahedral sites than an FCC crystal. However, the size of these interstitial sites in an FCC crystal is d = 0.414D (d is the interstitial void size and D is the diameter of the solvent atom), whereas the corresponding size in a BCC crystal is d = 0.155D. In general, the size of the interstitial atoms is greater than the interstitial site size. So the addition of interstitial atoms always creates a strain in the lattice. Since the size of the interstitial sites in an FCC crystal is larger than that in a BCC crystal, the concentration of impurities (except hydrogen) in an FCC crystal is typically higher than in a BCC crystal. This is the reason why the carbon concentration in an α-iron (BCC structure) is much less than in a γ-iron (FCC structure).

Another important difference between BCC and FCC lattices in terms of interstitial atoms is that in a BCC lattice, the occupation of the octahedral lattice site (Fig. 2.8) leads to distortion (due to the asymmetry of the octahedral site) and, consequently, to formation of a shear stress field around the interstitial. This enables the screw component (see Sect. 2.5.2) of the

dislocations (which possesses only the shear stress component) to interact with the stress field created. As in iron, for instance, at low temperatures, the majority of dislocations are of the screw type (or have the majority of the screw component), and this leads to differences in the mechanical properties of the BCC and FCC forms of iron.

2.5.2 Linear Defects

Dislocations, which are the most typical linear (or one-dimensional) defects, and their ability to move define the ductility (plasticity) of metals and explain why the strength of a metal crystal is far less than the theoretical strength calculated on the basis of the bond strength between the metal atoms. During typical plastic deformation, dislocations are formed by the Frank-Read source with the rate of $\sim 10^6$/s. Due to the force (stress), the dislocations glide along the close-packed crystal planes. When the dislocation density of a material is increased, also the internal energy is increased more than the entropy. Therefore, the dislocations are not stable and tend to annihilate or escape from the crystal. The decrease in ductility and increase in strength are related to the interactions between the dislocations as well as between the dislocations and other obstacles to movement such as precipitations or grain boundaries. At high homologous temperatures ($T > 0.45\ T_m$), dislocations can also climb, which increases the degrees of freedom of movement, leading to lower strength and higher ductility. In addition, many different types of crystals react at increased rates at the points where dislocations intersect the surface.

Even though the plastic deformation occurring via dislocation movement is qualitatively fully comprehended in macro- and microcrystalline materials, the quantitative analyses still remain incomplete [5]. This is due to the difficulties in averaging the interactions between dislocations and the other mechanisms contributing to the plastic flow on the plastic flow on the nanoscale, such as grain rotation, twinning, etc. [5]. It is also to be noted that, from an atomistic point of view, the length of dislocation becomes increasingly important as the grain size of the material approaches the nanoscale.

Although there are many different types of dislocations, they all can be considered as combinations of the two fundamental types (i.e., the edge dislocations and screw dislocations shown in Fig. 2.9).

Summary of dislocations:

1. Dislocations are formed during deformation.
2. Dislocations glide due to a stress (force) along close-packed planes running in a close-packed direction.

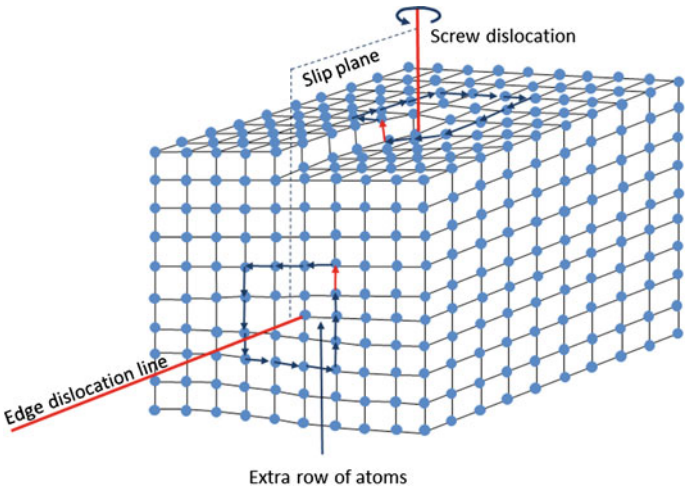

Fig. 2.9 Edge dislocation and screw dislocation

3. As dislocation density increases, the internal energy of the material increases more than its entropy. Therefore, dislocations are not stable and try to annihilate.
4. Dislocations interact with each other, and thus, gliding becomes more difficult. This, in turn, increases the strength of the material, yet the ductility is decreased. Other obstacles, such as grain boundaries and precipitates, have a similar effect.
5. At increased temperatures ($T > 0.45\ T_m$), dislocations can climb, which increases the degrees of freedom for their movement. This causes decrease in strength and increase in ductility.

2.5.3 Two-Dimensional Defects

The two-dimensional defects (i.e., planar defects, especially surfaces and interfaces) have a significant effect not only on the mechanical properties of materials but also on their chemical reactivity. For example, the reaction rates during corrosion are typically determined by the amount of exposed surface area. In addition, these defects, such as grain boundaries between crystallites in a polycrystalline alloy, provide lower activation energy short circuit paths for atomic diffusion and impurities tend to segregate there. Since the surface and interfacial diffusion can be orders of magnitude faster than that of bulk diffusion, see Fig. 10.2 in Chap. 10

Table 2.3 Lattice, grain boundary, and surface interdiffusion coefficients of Cu, Al, and $(SnPb)_{eut}$ at 100 °C [6]

Material	Temp. ratio 373/T_m	Diffusivities at 100 °C (m^2/s)
Cu	0.275	Lattice $D_l = 7 \times 10^{-24}$ Grain $D_{gb} = 3 \times 10^{-11}$ Surface $D_s = 10^{-8}$
Al	0.4	$D_l = 1.5 \times 10^{-15}$ $D_{gb} = 6 \times 10^{-7}$
$(SnPb)_{eut}$	0.82	$D_l = 2 \times 10^{-5 \text{ to } -6}$

these short circuit paths may have significant technological impacts, for example, in the electromigration reliability of electronic circuits, as can be seen from Table 2.3. In addition, the two-dimensional defects interact with other defects, such as dislocations, as discussed in Sect. 2.5.2.

It is also to be noted that these defects have their own energy, surface energy, which quantifies the disruption of intermolecular bonds that occur when a surface is created. The minimization of surface energy provides a driving force for many important phenomena such as sintering, wetting, and grain coarsening. Other types of planar defects are low- and high-angle grain boundaries, in which adjacent grains can be distinguished depending on the misalignments of atomic planes, twin boundaries, and antiphase boundaries.

2.5.4 Volume Defects

Volume defects (bulk defects, 3D defects) like precipitates, inclusions, cracks, voids, and pores also have important effects on the mechanical, thermal, electronic, and optical properties of solids. These defects are typically introduced into the material during manufacturing and fabrication steps. Furthermore, these defects are capable of increasing mechanical stress locally and are thus especially deleterious to the mechanical reliability of the metal. However, in dispersion hardening, foreign particles or additional elements that form precipitates are added to strengthen the parent material by forming obstacles to movement of dislocations facilitating plastic deformation. The good high-temperature strength of many super-alloys is due to the second-phase particles. Nonetheless, pores, cracks, and voids that act as stress concentration sites are typically detrimental for mechanical strength.

2.6 Some Examples of Intermediate Phases and Their Crystal Structure

There are numerous different kinds of ordered phases that are present with many differing crystal structures varying from being relatively simple to extremely complicated. There are basically two types that intermediate phases can form,

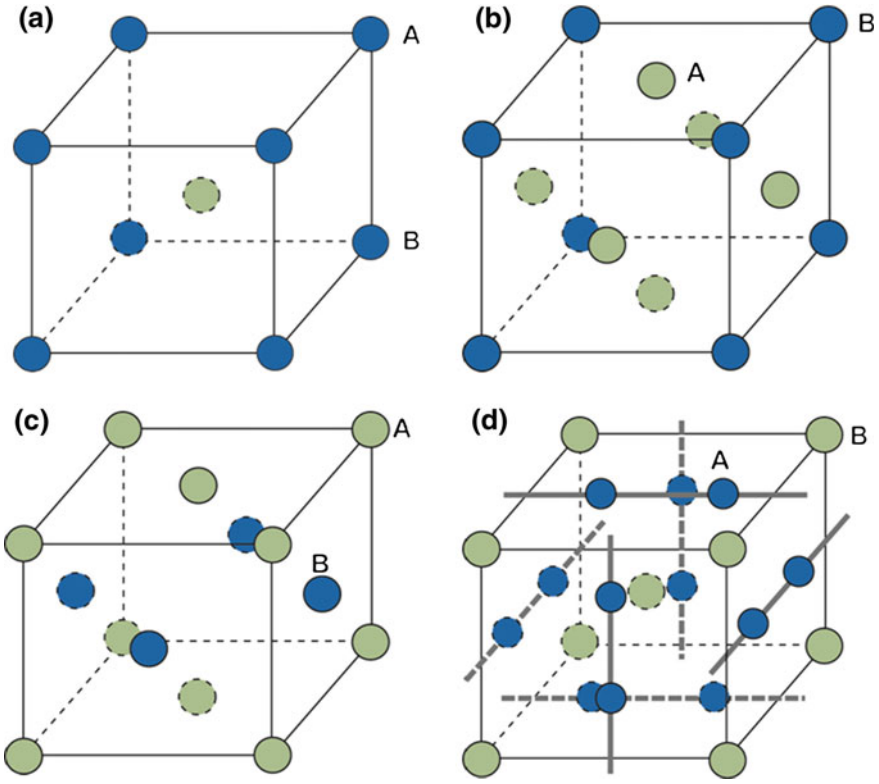

Fig. 2.10 Crystal structure of substitutional ordered phases: **a** B2 (AB)-NiAl, CoAl, CuZn, AuZn; **b** $L1_2$ (A_3B)-Ni_3Al, Ni_3Ga, Ni_3Ge; **c** $L1_o$ (AB) −CuAu, CoPt, FePt; **d** A15 (A_3B)- Nb_3Sn, Nb_3Ge, V_3Si

being interstitial and substitutional compounds. The precise type of phase that will form depends on the relative atomic size, valency, and electronegativity as was discussed earlier (Sect. 1.12). When one type of atom is much smaller than another, then the smaller atoms are able to occupy the interstitial positions in the crystal of the other atom. For example, different kinds of metal carbides are interstitial intermetallic compounds. Some of the examples are shown in Fig. 2.10. When atom sizes differ by a factor of 1.1–1.6, Laves phase might form (see Fig. 2.11). The other type are substitutional compounds where one type of atom occupies one particular sublattice and another type of atom occupies the other sublattice.

The main difference with these kinds of substitutional alloys and the case of random alloys is that there is an equal probability for both atoms to occupy a particular position. A few different examples of these kinds of compounds are shown in Fig. 2.10. Note that we have shown relatively simple examples which will be considered for discussion in forthcoming chapters. Some systems, for example, Cu_3Au, CuAu, and CuZn, transform to disordered phases at high temperature, because of the dominating role of entropy compared to enthalpy in these systems.

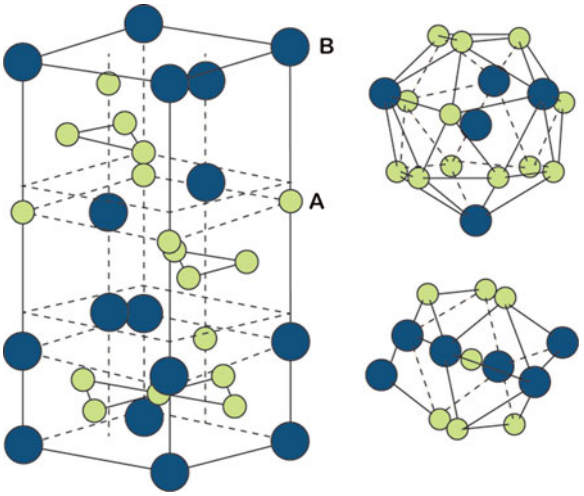

Fig. 2.11 C15 Laves phase A_2B type

2.6.1 Defects in Intermediate Phases

The composition range of the intermediate phases in binary systems can vary from a very narrow homogeneity range, as shown in Fig. 1.26, to a reasonably wide homogeneity range, as shown in Fig. 1.27. There is no ordered phase present which is a perfect line compound that is with stoichiometric composition without any deviation. The deviation from stoichiometric composition is achieved by the presence of constitutional defects in the structure. Mainly two types of defects are found in these structures. One type is structural vacancies. Note that structural vacancies found because of deviation from the stoichiometric composition are different from the thermal vacancies which are always present at a specific temperature with a certain equilibrium concentration. Another type of defect which is typically found is an antisite (or an antistructure) defect that is created when an atom occupies a position belonging to the other type of atom.

To clarify what has been stated above, let us consider one of the most studied ordered structures, the B2 phase. Let us see the crystal structure a little differently, as shown in Fig. 2.12a. The lattice positions can be divided into two types, the α- and β-sublattices. If A atoms, in a binary A–B alloy, occupy the α-sublattice ([0,0,0] positions), then the B atoms will occupy the β-sublattice ($[\frac{1}{2}, \frac{1}{2}, \frac{1}{2}]$ positions). It can be seen that two simple cubes of the α-sublattice and the β-sublattice interpenetrate each other forming the B2 structure. At stoichiometric composition and in a perfect crystal, we expect this condition to occur. However, when composition deviates from the stoichiometric composition, defects will be present in the structure and the number of defects depends on the extent of deviation in the composition.

There can be two types of B2 intermediate phases. One type is in the A-rich side where antisite defects are present, whereas in the B-rich side, triple defects are present, as shown in Fig. 2.12. A triple defect is so named because it comprises a total

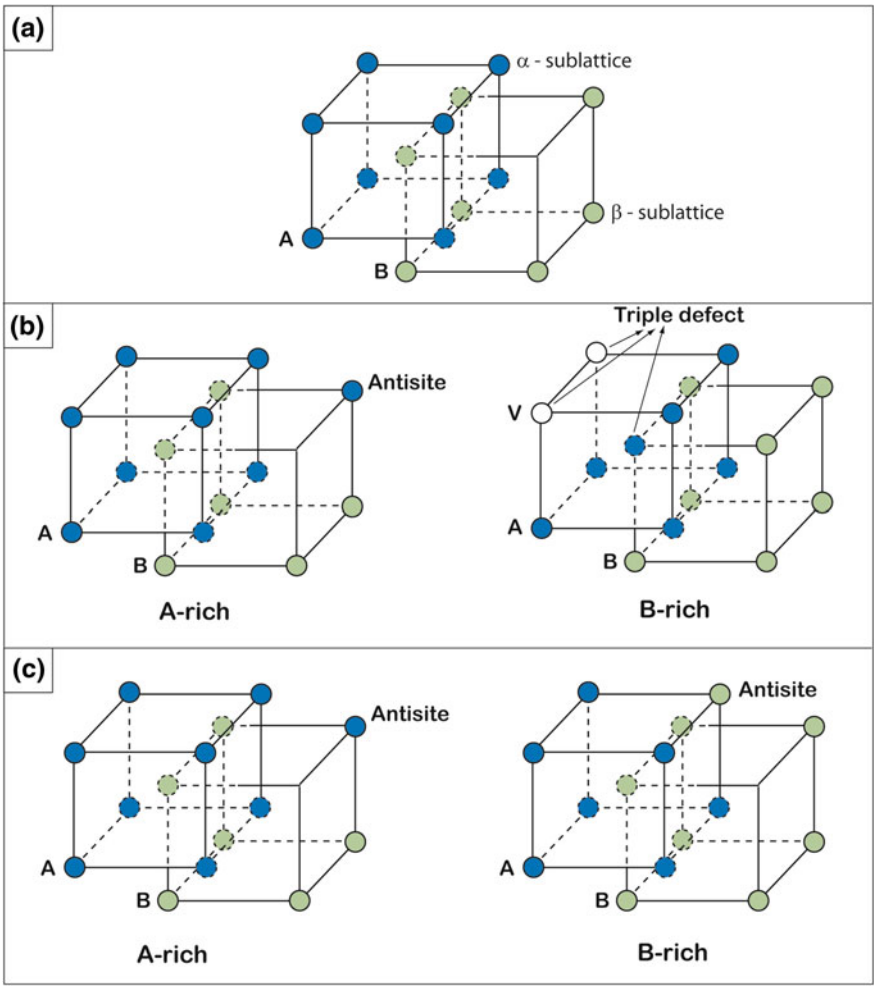

Fig. 2.12 Defect structure in B2 phases. **a** Perfect crystal. **b** Phases where on one side of the stoichiometric composition, there is the presence of triple defects, whereas on the other side, antisite defects are present. **c** Phases where on both sides of the stoichiometric compositions, antisite defects are present

of three defects, namely two vacancies in the α-sublattice and one antisite defect in the β-sublattice. It is important to keep in mind that the triple defects are not necessary bounded defects, i.e. the vacancies and antisite do not necessary occupy nearest neighboring positions. The triple defect disorder refers the *total* defect concentrations when there are two vacancies for each antisite atom, see Sect. 2.6.3 for more details. These kinds of defects are found, for example, in the B2 NiAl, CoAl, NiGa, and CoGa phases. There is another kind of B2 phase, where in both sides of the stoichiometry, only antisite defects are present, as shown in Fig. 2.12c. This kind of defect is found in the B2 AuZn, CuZn, AgZn, and AgMg phases, for instance.

However, it should be pointed out that a triple defect is not a common defect in phases other than the B2 structure. Instead, simple vacancies are typically present. Moreover, in most of the ordered phases in both sides of the stoichiometry, only antistructure defects are present. We have seen earlier that at above 0 K, there will always be some vacancies present (their number depending on the temperature) due to the fact that they are thermodynamic equilibrium defects. Similarly, in ordered phases, even at stoichiometric composition vacancies and antistructure, defects will be present and the number of defects increases with increasing temperature. However, calculation of point defects in ordered phases is not very straightforward as shown next.

2.6.2 *Crystal Structures and Point Defects in Ordered Binary Intermetallics on an Example of Ni-, Ti-, and Fe-Aluminides*

The ordered Ni-, Ti-, and Fe-aluminides reveal different crystalline structures. The most important are the following: B2 (NiAl and FeAl, see Fig. 2.10a), $L1_2$ (Ni_3Al, see Fig. 2.10b), $L1_0$ (TiAl, see Fig. 2.10c), $D0_{19}$ (Ti_3Al, see Fig. 2.13a), and $D0_3$ (Fe_3Al, see Fig. 2.13b). Here, the ideally ordered crystalline structures of Ni-, Ti-, and Fe-aluminides are schematically presented, i.e., the structures at zero temperature and at perfect stoichiometric compositions. As the temperature increases and/or the composition deviates from stoichiometry, substitutional point defects are inevitably generated. Four types of substitutional point defects can generally be introduced in a two-atomic intermetallic compound AB, namely the vacancies on both sublattices, V_A and V_B, and the atoms on the differing sublattices, A_B and B_A (the antistructure or antisite atoms). One may differentiate between *structural* (constitutional) and *thermal* point defects which could be created in an off-stoichiometric intermetallic compound. In a strict definition, the structural defects are those defects which remaining thermal equilibrium in the intermetallic compound even at $T = 0$ in its maximally ordered state in order to accommodate the deviation from the stoichiometric composition. The difference between the real concentration of defects at $T \neq 0$ and the concentration of the structural defects presents the concentration of the thermal defects.

In a strict sense, nature does not "mark" the defects as constitutional or thermal ones. Such subdivision is helpful only from an educational point of view in order to refer to different sources of defects in a given compound. In such a definition, the concentration of thermal defects can even be *negative*. The Al-rich phase NiAl seems to present such an example. A further difference between the structural and thermal defects stems from the fact that one type of structural point defects is generally sufficient to accommodate the deviation from the stoichiometry, whereas at least two types of thermal point defects have to be simultaneously created to satisfy the mass-balance conditions (to preserve the given composition, i.e., the given ratio between the constitutional elements).

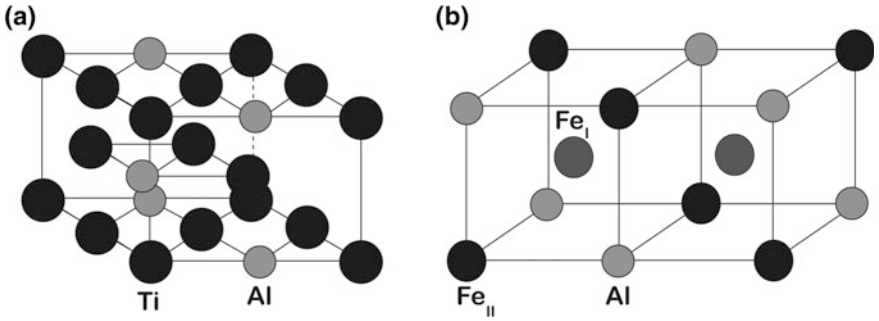

Fig. 2.13 Lattice structures of Ti_3Al **a** and Fe_3Al **b** aluminides. The Ti and Al atoms are represented by *black* and *gray* spheres. Fe has two sublattices indicated by Fe_I and Fe_{II}

Moreover, the point defects have not to be uniformly distributed over the different sublattices in an ordered intermetallic compound.

In Fig. 2.14, the concentrations of different defects in the intermetallic compounds under consideration are compared at $T = 0.75T_m$. This temperature corresponds to $T = 1{,}252$ K for Ni_3Al, 1,434 K for NiAl, 1,457 K for Ti_3Al, 1,294 K for TiAl, and 1,195 K for FeAl. T_m is the melting temperature of the stoichiometric composition of the given compound. The defect concentrations on different sublattices can be calculated according to the chemical reaction approach described below. Since in an intermetallic compound, point defects are created in a correlated manner in order to preserve the given composition, the concentration of point defects depends on the formation energies of all four types of defect. The literature data were here used for numerical estimates. It is important to note that the formation entropy effects were neglected.

The chemical reaction approach is outlined below for the example of NiAl. The vibrational energy contribution is neglected.

2.6.3 Calculation of Point Defect Formation Energies

The calculation of defect energies in pure metals is quite straightforward and was presented in Sect. 2.5 in detail. In the case of intermetallic compounds, however, the defect energies have to be calculated in a modified way. The energy difference between a block of perfect unit cells and that containing a given defect yields the values which may be called the "raw" formation energy of the defect. The "raw" values of single defects together with the cohesive energy per atom, ε_0, used in the presented estimates, are listed in Table 2.4. The B2 NiAl phase is exemplified here as a binary AB compound (A = Ni and B = Al). Since introduction of a single defect generally violates the composition of the compound, these "raw" values by themselves cannot represent the thermodynamical quantities. The effective formation energies, which correspond to the Arrhenius approximations of the temperature dependence of the defect concentrations, can be used with this aim.

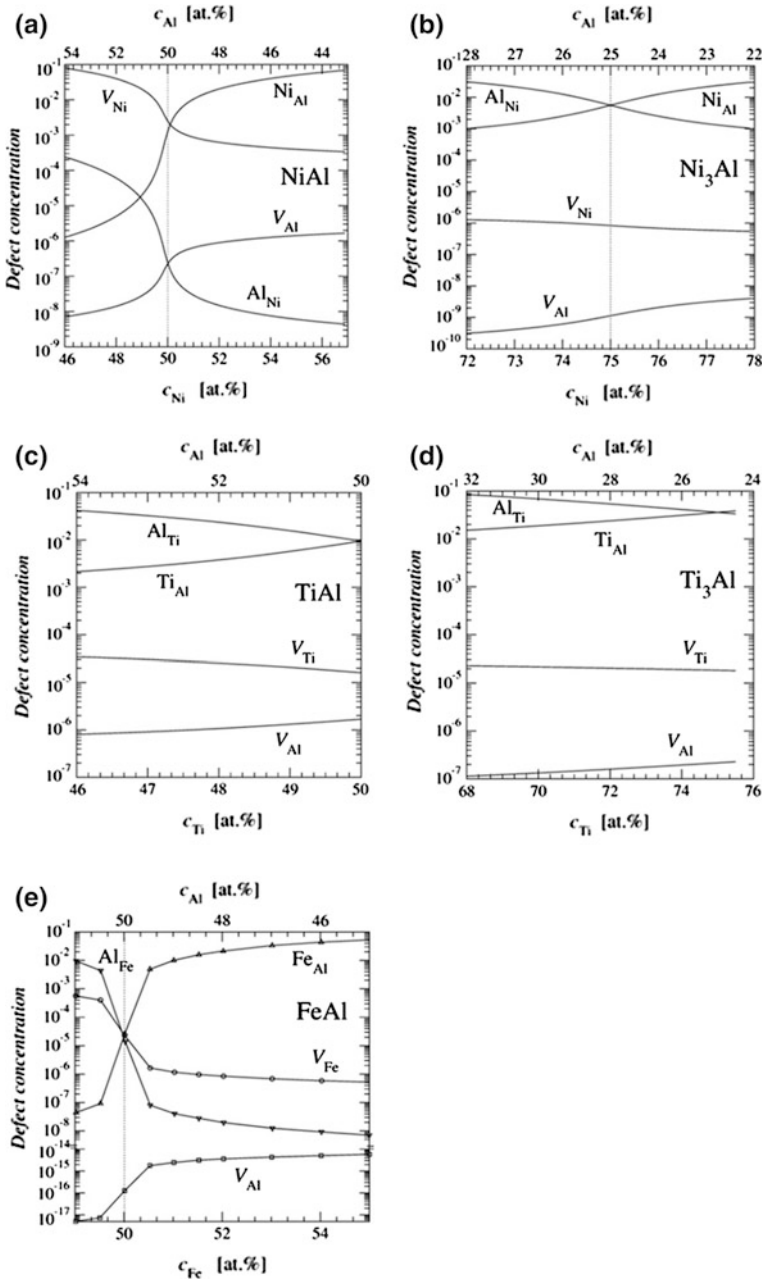

Fig. 2.14 Concentrations of vacancy and antistructure atoms on transition metal and aluminum sublattices in NiAl, Ni_3Al, TiAl, Ti_3Al, and FeAl as a function of composition at $T = 0.75\ T_m$ (T_m is the melting point of the compound)

Table 2.4 The "raw" formation energies of single point defects in NiAl where V is the vacancy, the bottom subscript denotes the sublattice, and ε_0 is the cohesive energy of the alloy

	$\varepsilon_{V\mathrm{Ni}}$	$\varepsilon_{V\mathrm{Al}}$	$\varepsilon_{\mathrm{Ni\_Al}}$	$\varepsilon_{\mathrm{Al\_Ni}}$	ε_0
"Raw" formation energy, eV/atom	5.978	5.471	−0.920	3.457	−4.494

The equilibrium defect concentrations in an intermetallic compound can be calculated using either canonical or grand canonical ensemble formalism. Of course, both methods will give the same result, so the choice of approach is a matter of convenience. Alternatively, the point defects can be treated as individual species and different point defect reactions can be considered as chemical reactions in a multicomponent lattice gas [7]. This approach is sketched here and, of course, it gives the same results as the previous two, yet in a slightly more elegant way.

Till the end of this section, we will use a special notation for the defect concentrations in view of a specific structure of an ordered compound. We will introducing the occupation probabilities of a defect P on a given sublattice denoted as Y_P instead of concentration variables, which are determined in mole fractions. This approach simplifies significantly the analysis for ordered compounds.

The point defect concentrations are assumed to be small, so that the defect interactions are neglected. Formally, each type P of point defects is described by a chemical potential

$$\mu_P = \varepsilon_P + kT \ln Y_P \tag{2.27}$$

Here, ε_P is the "raw" formation energy of a single defect and Y_P is the occupation probability of the defect P per unit site in its own sublattice. The commonly used defect concentrations, X_P, see Sect. 2.5, expressed as the site fractions of the number of defects are related to Y_P by the obvious relation for the B2 structures: $2X_P = Y_P$.

The four unknown equilibrium point defect concentrations $\{Y_P\}$ in a B2 compound, i.e., the vacancy concentrations on the two sublattices and the concentrations of the two types of antisite atoms, can be determined from the kinetic equilibrium conditions with respect to the three point defect reactions, supplemented by the conservation law for a fixed alloy composition. The latter can be written in the form

$$\xi(1 - 2Y_{V_\mathrm{A}} - 2Y_{V_\mathrm{B}}) = \frac{1}{4}(Y_{V_\mathrm{B}} - Y_{V_\mathrm{A}}) + \frac{1}{2}(Y_{\mathrm{A_B}} - Y_{\mathrm{B_A}}) \tag{2.28}$$

where

$$\xi = X_\mathrm{A} - \frac{1}{2} \tag{2.29}$$

is the deviation of the alloy composition (mole fraction of A, $\mathrm{X_A}$) from the ideal stoichiometric composition ($X_\mathrm{A} = 0.5$). Neglecting the terms such as ξ^2 in

Eq. 2.28 for small deviations from the stoichiometric composition and small concentrations of the point defects, the above equation can be presented as

$$\xi = \frac{1}{4}(Y_{V_B} - Y_{V_A}) + \frac{1}{2}(Y_{A_B} - Y_{B_A}) \tag{2.30}$$

The choice of three point defect reaction is a matter of convenience and depends on whether we deal with a triple-defect or antisite disorder compound. For the NiAl alloy, for instance, a convenient set of reactions is

$$2V_A + A_B + AB \leftrightarrow 0 \tag{2.31}$$

$$A_B + B_A \leftrightarrow 0 \tag{2.32}$$

$$2V_B + AB \leftrightarrow A_B \tag{2.33}$$

Equation 2.31 represents the triple-defect equilibrium in the system. It simply shows that a triple defect can be cancelled by adding a structural unit AB to the system. Similarly, Eq. 2.32 represents an antisite equilibrium and shows that a pair of antistructure atoms can be created or cancelled. Finally, Eq. 2.33 shows that, if we initially have two B vacancies and add a structural unit NiAl, then Al will cancel one of the vacancies, while Ni will turn the other vacancy into an Ni_{Al}-antistructure atom.

The dynamic equilibrium in the above defect reactions, Eqs. 2.31–2.33, can be reached by the equality of corresponding chemical potentials. The structural unit, NiAl, will be presented by $2\varepsilon_0$. This will give

$$\varepsilon_t d + kT \ln Y_{V_A}^2 Y_{A_B} = 0 \tag{2.34}$$

$$\varepsilon_{A_B} + \varepsilon_{B_A} + kT \ln Y_{A_B} Y_{B_A} = 0 \tag{2.35}$$

$$2\varepsilon_{V_B} - \varepsilon_{A_B} + 2\varepsilon_0 + kT \ln\left(\frac{Y_{V_B}^2}{Y_{A_B}}\right) = 0 \tag{2.36}$$

Here, $\varepsilon_{td} = 2\varepsilon_0 + 2\varepsilon_{V_A} + \varepsilon_{A_B}$ is the so-called triple-defect energy.

Equations 2.30 and 2.34–2.36 could be solved numerically for the four defect concentrations in dependence on the composition of the alloy. Then, the effective activation energies can be estimated by linear fitting in the logarithm concentration against the inverse temperature coordinates within the given temperature interval. The analysis shows that the temperature dependence of the point defect concentrations can be adequately treated with a single formation energy. The specific results for NiAl are given in Fig. 2.15.

Besides that, Eqs. 2.30 and 2.34–2.36 can be solved analytically in an approximate manner by using the fact that in NiAl, Y_{V_A} and Y_{A_B} are much greater than the other two concentrations. Then, Eq. 2.30 can be rewritten in the form

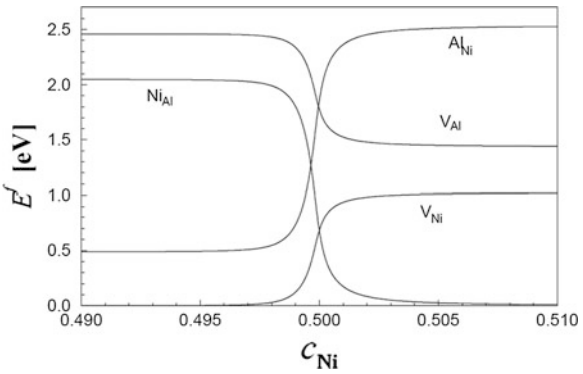

Fig. 2.15 Effective formation energies E^f of the point defects as function of composition c_{Ni}

$$\xi = \frac{1}{2} Y_{A_B} - \frac{1}{4} Y_{V_A} \tag{2.37}$$

From Eq. 2.37, we have $Y_{V_A} = 2Y_{A_B}$ for the stoichiometric composition, $\xi = 0$. For the A-rich compositions $\xi > 0$, the A antistructure atoms are the main defects $(Y_{V_A} \ll Y_{A_B})$ and Eq. 2.37 transforms into $Y_{A_B} = 2\xi$. On the other hand, for the B-rich compositions $\xi < 0$, the A vacancies are mainly formed $(Y_{V_A} \gg Y_{A_B})$ and Eq. 1.174 will be read as $Y_{V_A} = -4\xi$. These relations make it possible to solve analytically the system of Eqs. 2.34–2.36 and to find the concentrations of all four point defects under the given approximations. The analytical expressions for the effective formation energies are given in Table 2.5. The comparison with Fig. 2.15 suggests that these results correspond well to the numerical data at the stoichiometric composition and far from the stoichiometry.

The calculations suggest that the Ni vacancies and the Ni antistructure atoms are the main defects in NiAl and the concentration of Al vacancies is by a few orders of magnitude lower than the concentration of Ni vacancies in accordance with the experimental observations.

A similar form of analytic solution can be used for other compounds, and the results are presented in Fig. 2.14. Figure 2.14a–e demonstrate a few important features of defect behavior. It is obvious that both the Ti-aluminides (Fig. 2.14c, d) and Ni_3Al (Fig. 2.14b) belong to the antistructure defect type of intermetallic compounds, since antistructure atoms are predominantly generated to accommodate the deviation from the stoichiometry. In contrast, NiAl reveals a triple-defect type of point defect disorder and constitutional Ni vacancies exist in NiAl on the Al-rich side, as in Fig. 2.14a. Moreover, the Ni vacancy concentration is very large also on the Ni-rich side, for example, $X_{V_A} \sim 10^{-4}$ at $T = 0.75T_m$. In the other intermetallics under consideration, the vacancies are also mainly concentrated on the transition metal sublattice and their concentration amounts to about 10^{-6} to 10^{-5} at $T = 0.75T_m$. These are also the typical vacancy concentrations in close-packed pure metals at the same reduced temperature. The vacancy concentration on the Al sublattice is remarkably smaller, especially in B2–FeAl, see Fig. 2.14e.

Table 2.5 Analytical expressions of the effective formation energies Q_P^f of the point defects P, $P = V_{Ni}$, V_{Al}, Ni_{Al}, and Al_{Ni} (in eV/Atom) in NiAl in dependence on composition $\xi = X_{Ni} - ½$

	$\xi < 0$	$\xi = 0$	$\xi > 0$
$Q^f_{V_{Ni}}$	0	$\varepsilon_{td}/3$	$\varepsilon_{td}/2$
	0	0.683	1.024
$Q^f_{V_{Al}}$	$2\varepsilon_0 + \varepsilon_{V_{Al}} + \varepsilon_{V_{Ni}}$	$(4\varepsilon_0 + 3\varepsilon_{V_{Al}} + \varepsilon_{V_{Ni}} - \varepsilon_{Ni_{Al}})/3$	$\varepsilon_0 + \varepsilon_{V_{Al}} - \frac{1}{2}\varepsilon_{Ni_{Al}}$
	2.461	1.778	1.437
$Q^f_{Ni_{Al}}$	ε_{td}	$\varepsilon_{td}/3$	0
	2.048	0.683	0
$Q^f_{Al_{Ni}}$	$\varepsilon_{Al_{Ni}} - 2\varepsilon_0 - 2\varepsilon_{V_{Ni}}$	$(-2\varepsilon_0 - 2\varepsilon_{V_{Ni}} + 3\varepsilon_{Al_{Ni}} + 2\varepsilon_{Ni_{Al}})/3$	$\varepsilon_{Al_{Ni}} + \varepsilon_{Ni_{Al}}$
	0.489	1.854	2.537

B2–FeAl is neither a compound with a pure antisite disorder nor a compound with a pure triple-defect disorder. FeAl demonstrates a hybrid behavior in which the relation between the Fe vacancy concentration and that of the antistructure atoms depends crucially on temperature.

The concentration of the Ti antistructure atoms in the Ti-aluminides is generally larger than that of the Ni antistructure atoms in the Ni-aluminides of the same composition, as in Fig. 2.14. This fact corresponds to a higher degree of thermal disorder inherent in Ti-aluminides at similar reduced temperatures. These features play a decisive role in the analysis of the respective self-diffusion behavior.

An important question now arises as to how the particular crystal structure of the given intermetallic compound can affect the self-diffusion properties. It is generally accepted that self-diffusion in close-packed structures occurs via nearest-neighbor jumps of vacancies. Since random vacancy jumps between different sublattices would generally produce disorder (and since there is a strong tendency to accomplish the reverse), ordering jump after a given disordering jump, the correlated jumps of vacancies will clearly play a decisive role in the long-range diffusion process. These problems will be considered in Chap. 5.

2.7 Microstructure and Phase Structure

The structural details at different levels that create the microstructure of a given material are shown in Fig. 2.16. On the other hand, microstructures can be divided, based on the formation mechanism, into three major types namely solidification structures, solid-state transformation structures, and annealing structures. Figure 2.17 shows, as an example, an eutectic solidification structure of AuSn-alloy and the same material after annealing at 150 °C for 6,600 h. A profound discussion on different types of microstructures can be found, for example, from the ASM handbook, and therefore, it is not included here [1] (Fig. 2.16).

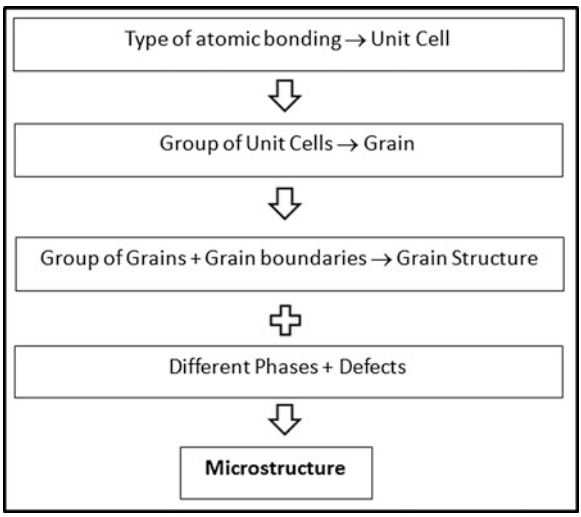

Fig. 2.16 Structural details at different levels creating the microstructure of a material

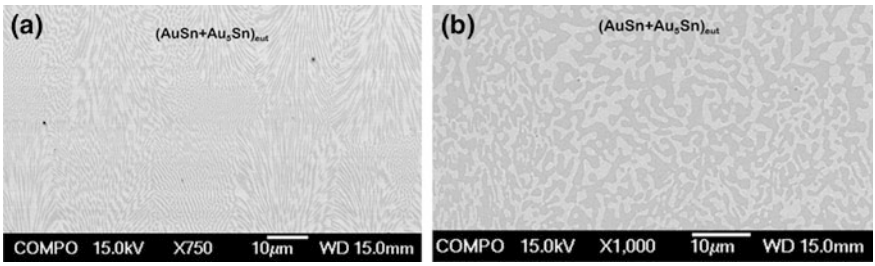

Fig. 2.17 **a** Eutectic solidification structure of Au80Sn20 (wt %) alloy and, **b** the same structure after annealing at 150 °C for 6,600 h

References

1. ASM Handbook, vol 9, Metallography and Microstructures, ASM International Materials Park Ohio, USA 2004.
2. W. D. Callister, Jr., D. G. Rethwisch, Materials Science and Engineering: An Introduction,John Wiley & Sons, Canada 2009.
3. R. Tilley, Understanding Solids-The Science of Materials, John Wiley & Sons, Chichester West Sussex, England 2006.
4. J. K. Kivilahti, Metalliseosten teoria: Tasapaino-ominaisuudet ja rakenne, Otakustantamo, 1982.
5. K.S. Kumar, H. Van Swygenhoven, S. Suresh, Mechanical behavior of nanocrystalline metals and alloys, Acta Materialia 51 (2003) 5743–5774.
6. K.-N. Tu, Solder Joint Technology: Materials, Properties, and Reliability, Springer, 2007.
7. Y. Mishin, C. Herzig, Diffusion in the Ti-Al system, Acta Materialia 48 (2000) 589–623.